Shap. Mem. Superelasticity (2023) 9:615–625
https://doi.org/10.1007/s40830-023-00462-w

ORIGINAL RESEARCH ARTICLE

The Influence of Aging on Shape Memory Effect in Ti-50.7at.%Ni and Ti-51.7at.%Ni Single Crystals

E. E. Timofeeva[1] · M. V. Zherdeva[1] · E. Yu. Panchenko[1] · A. S. Eftifeeva[1] · N. Yu. Surikov[1] · A. I. Tagiltsev[1] · Yu. I. Chumlyakov[1] · E. S. Marchenko[1]

Received: 27 June 2023 / Revised: 31 July 2023 / Accepted: 17 August 2023 / Published online: 1 September 2023

Abstract The shape memory effect (SME) during stress-assisted thermal cycles under compressive load in [001]-oriented Ti-50.7at.%Ni and Ti-51.7at.%Ni single crystals aged at 823 K for 1 h has been studied. Ti_3Ni_4 particles with a diameter of 300–400 nm were precipitated with volume fractions of 11 and 22% and interparticle distances of 300–500 nm and 50–150 nm, respectively. In quenched single crystals, the SME parameters were determined by the transformation type (thermal-induced martensitic transformation (MT) or strain glass transition). In contrast, the SME parameters of aged single crystals were determined by the volume fraction of particles and interparticle distances. Differing volume fractions of particles and interparticle distances led to different temperatures (M_s^0) for the formation of B19′-martensite, different strain (ε_{rev}), different dependences of the interval of forward MT (Δ_1^σ) and thermal hysteresis ($\Delta T_1^\sigma = A_f^\sigma - M_s^\sigma$ and $\Delta T_2^\sigma = A_s^\sigma - M_f^\sigma$) on applied stresses, and changes in the morphology of martensite crystals. Practically, these differences do not affect the stresses (σ_{min} and σ_{max}) required to achieve the minimum strain and maximum reversible strain (ε_{rev}) and strain growth coefficient ($d\varepsilon_{rev}/d\sigma$). The influence of aging on the dependence of the SME parameters on the chemical composition was analysed in comparison with quenched crystals.

Keywords Shape memory effect · TiNi single crystals · Aging · Strain glass transition

✉ E. E. Timofeeva
timofeeva_katie@mail.ru

[1] Tomsk, Russia

Introduction

The thermoelastic B2–B19′ martensitic transformations (MTs) in quenched [001]-oriented Ti-50.7at.%Ni and Ti-51.7at.%Ni single crystals were studied in [1]. Thermal-induced B2–B19′ MT (Ti-50.7at.%Ni), or strain glass transition (Ti-51.7at.%Ni) determined the following shape memory effect (SME) parameters: the morphology of the martensite structure in the stress-assisted cooling/heating cycles; stress σ_{app} for oriented martensite formation during stress-assisted cooling/heating cycles; and the coefficient $d\varepsilon_{rev}/d\sigma$, which determines the strain dependence on the stress $\varepsilon_{rev}(\sigma_{app})$. The main factor that caused the difference is the ability of Ti-50.7at.%Ni single crystals to form a special martensite structure during stress-assisted cooling/heating cycles [2]. This is a mixture of thermal-induced self-accommodating structure and stress-induced oriented martensite. In contrast, the thermal-induced martensite did not appear in the Ti-51.7at.%Ni crystals, and, accordingly, there is no such martensite mixture [1].

It is known [3, 4], that in a strain glass TiNi alloy with a high nickel content (more than 51.2at.%), it is possible to obtain thermal-induced MTs due to aging, leading to the precipitation of large Ti_3Ni_4 particles (300–400 nm in size) and providing a decrease in the nickel content of the matrix. If quenched Ti-50.7at.%Ni and Ti-51.7at.%Ni alloys undergo a different type of transition in cooling/heating cycles, then aged alloys undergo the same type of transition-thermal-induced MT. Moreover, the different chemical composition of the matrix in Ti-50.7at.%Ni and Ti-51.7at.%Ni alloys becomes closer after aging due to the precipitation of a different volume fraction of particles (tends to Ti-50.4–50.6at.%Ni) [5, 6]. Consequently, in aged alloys one should expect the degeneration of the

strong dependence of the SME parameters on the chemical composition, which was typical for quenched alloys.

However, it is impossible to predict how strongly the SME dependence on the initial chemical composition will degenerate in aged alloys for the following reasons. Different chemical composition of quenched alloys leads to different volume fraction of particles and different interparticle distances [7]. A different volume fraction of particles in Ti-50.7at.%Ni and Ti-51.7at.%Ni alloys causes the different values of the reversible strain, since the particles do not undergo MT [8]. A strong decrease in interparticle distances can change the mechanism of nucleation and propagation of martensite [9], which can lead to a change in SME parameters, such as temperature intervals of MT and hysteresis. Indeed, as shown in [10], in [111]-oriented Ti-50.1at.%Ni and Ti-51.5at.%Ni single crystals, aged at 823 K for 1.5 h, different dependences of thermal hysteresis on tensile stresses were observed. Hence, the dependence of the SME parameters on the chemical composition can intensify after aging. Thus, the aging of TiNi alloys with different chemical composition provokes the appearance of opposite factors, leading both to degeneracy of the chemical composition dependence of the SME parameters and to an intensification of this dependence.

Despite the large amount of studies focused on the SME in TiNi alloys, there are no works aimed on the effect of aging on the dependence of SME parameters on different chemical compositions in TiNi single crystals. Most of the research within this topic mainly reveals the effect of thermomechanical treatment on the SME strain, the MT temperature, etc. and conducted on polycrystals. The grain boundaries in polycrystals are the sites of predominant precipitation of particles [11–13]; the particle's volume fraction can vary inside the grain [13, 14]. Therefore, it is more expedient to choose single crystals for the research. But the studies deal with TiNi single crystals mainly includes only orientation dependence of the SME for various particle sizes [3, 10, 15]. At the same time, the high-strength [001]-orientation under compression has been studied very poorly.

The foregoing facts determine the relevance of the present work devoted to the study the SME parameters during stress-assisted cooling/heating in Ti-50.7at.%Ni and Ti-51.7at.%Ni single crystals, aged at 823 K, 1 h, and the elucidation of the aging effect on the chemical composition dependence of SME parameters. We will show which dependence of SME parameters on the chemical composition will degenerate, and which will intensify after aging. The microstructural mechanisms that determine these effects will be considered. The role of the volume fraction of Ti_3Ni_4 particles and the interparticle distances in determining the SME parameters will be elucidated.

Materials and Methods

Single crystals of Ti-50.7at.%Ni and Ti-51.7at.%Ni single crystals were grown by the Bridgman method. The high-strength < 001 > orientation was chosen for compressive load testing. As-grown single crystals were subjected to high-temperature annealing at 1253 K for 1 h, followed by quenching in water to obtain the single-phase structure. Next, the quenched crystals were aged at 823 K for 1 h, followed by quenching.

The MT temperatures were investigated from calorimetric curves obtained using a differential scanning calorimeter (DSC 404 F1) and from the temperature dependence of the electrical resistance. Mechanical tests were conducted on a dilatometer during stress-assisted cooling/heating cycles to obtain the ε(T) curves. The samples for compression had a parallelepiped shape with dimensions of $3\times3\times6$ mm. During the stress-assisted cooling/heating cycles next SME parameters were obtained from the ε(T) curves [15–17]: the M_s^σ temperature; the forward and reverse MT intervals, $\Delta_1^\sigma = M_s^\sigma - M_f^\sigma$, $\Delta_2^\sigma = A_f^\sigma - A_s^\sigma$; two hysteresis values, $\Delta T_1^\sigma = A_f^\sigma - M_s^\sigma$ and $\Delta T_2^\sigma = A_s^\sigma - M_f^\sigma$; reversible strain ε_{rev}, the stresses σ_{min} required to obtain the minimum reversible strain ε_{rev} with value 0.3–0.5% no less than measurement error 0.2%; the stresses σ_{max} required to obtain the maximum reversible strain ε_{rev}; the coefficient $d\varepsilon_{rev}/d\sigma_{app}$, describing the growth of strain with stress. Electron microscopy was performed using an HT-7700 Hitachi. During data analysis, the average measurement errors were: for strain ± 0.2%, for temperature ± 2 K, and for stress ± 2 MPa.

Experimental Results

Figure 1 shows the microstructure of the aged Ti-50.7at.%Ni and Ti-51.7at.%Ni single crystals. Aging at 823 K for 1 h led to the precipitation of four variants of Ti_3Ni_4 particles. The particle size weakly depends on the chemical composition and varies within 300–400 nm, as reported in [18]. However, the interparticle distance and volume fraction of the particles differed significantly. The volume fraction of particles increased from 11 to 22% with an increase in the Ni content from 50.7 to 51.7 at.%. This led to a decrease in the average interparticle distance from 300–500 to 50–150 nm.

In aged single crystals, the MT from the B2-phase to B19′-martensite passes through the R-phase. The B2-R-B19′ MT temperatures (M_s^0, M_f^0, A_s^0, A_f^0, T_R) during stress-free cooling/heating in aged crystals are represented in Table 1 as well as the forward MT interval, $\Delta_1^0 = M_s^0 - M_f^0$, the reverse MT interval, $\Delta_2^0 = A_f^0 - A_s^0$, and two hysteresis values, $\Delta T_1^0 = A_f^0 - M_s^0$ and $\Delta T_2^0 = A_s^0 - M_f^0$.

The two-stage transformation B2-R-B19′ is a typical of all aged TiNi alloys with dispersed Ti_3Ni_4 particles [3, 8, 9,

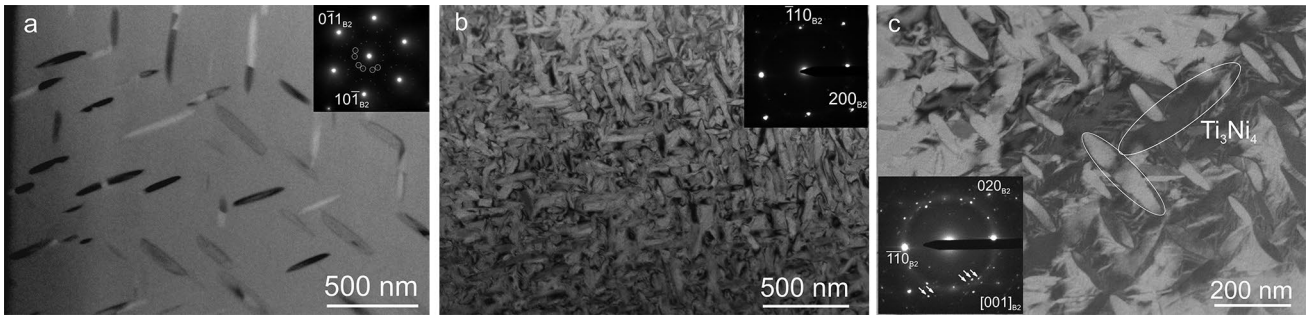

Fig. 1 Microstructure of aged single crystals: **a** Ti-50.7at.%Ni single crystal, reflexes of Ti_3Ni_4 particles are marked by circles; **b**, **c** Ti-51.7at.%Ni single crystal, reflexes of Ti_3Ni_4 particles are marked by arrows

18, 19]. The MT temperatures for aged Ti-51.7at.%Ni single crystals were lower than for Ti-50.7at.%Ni single crystals. The first reason for this may be the different Ni contents in the matrix following the precipitation of different volume fractions of Ni-enriched Ti_3Ni_4 particles. The decreased Ni content of the TiNi binary alloys increases the M_s^0 temperature by ~ 16–18 K per 1 at. % of Ni [8]. The second reason is small interparticle distances in Ti-51.7at.%Ni single crystals, described in detail in Sect. "Discussion".

The forward and reverse MT intervals, Δ_1^0 and Δ_2^0, two hysteresis values, ΔT_1^0 and ΔT_2^0 also strongly vary for Ti-50.7at.%Ni and Ti-51.7at.%Ni single crystals. In Ti-51.7at.%Ni single crystals, the MT occurred in a wide temperature range $\Delta_1^0 = 87$ K, in contrast to Ti-50.7at.%Ni crystals, where the MT interval $\Delta_1^0 = 36$ K is 2.5 times smaller. The hysteresis ΔT_2^0 is 3 times wider in Ti-51.7at.%Ni compared with Ti-50.7at.%Ni single crystals.

Figure 2 shows the ε(T) curves for aged crystals during stress-assisted cooling/heating cycles. In aged single crystals, B2-R-B19′ MTs were observed during cooling at low stresses and B2–B19′ MTs at high stresses. However, all ε(T) curves had a single stage. The stage associated with the R-transformation is absent in the ε(T) curves because the strain during the B2-R transition is zero along the [001]-direction, and the stress applied along the [001]-direction does not affect the morphology of R-martensite [19, 20]. In other words, the same R-martensite variants arise during stress-assisted cooling as during stress-free cooling. They are elastically accommodated, and there are no macroscopic changes in the dimensions of the sample. Thus, during cooling under low stress the B2-R transformations observed at T_R without any macroscopic strain. Subsequent cooling induced the R-B19′ transition with macroscopic strain on condition, that start temperature M_s^σ was lower than T_R. This condition was realized at stresses of 0–100 MPa in Ti-50.7at.%Ni crystals and 0–300 MPa in Ti-51.7at.%Ni. It should be noted that the temperature M_s^σ grows significantly with increasing stress, but temperature T_R changes lightly [15]. So, at specified stress M_s^σ became higher than T_R. If $M_s^\sigma > T_R$ at higher stress, then B2–B19′ MT occurred and there was no R-transformation. Such situations were observed at stresses above 100 MPa in Ti-50.7at.%Ni and above 300 MPa in Ti-50.7at.%Ni. Thus, only one stage in the ε(T) curves was obtained independently of transformation type (R-B19′ or B2–B19′) providing the macroscopic strain. A similar effect has been observed in many studies of TiNi alloys when the strain associated with the stress-induced R-transformation was absent on the ε(T) curves in [001]-oriented single crystals [1, 2, 9, 15, 19, 20]. When single crystals were compressed along other orientations or polycrystals, the R-transformation was observed in the ε(T) curves [15, 18].

The σ_{min} and σ_{max}, required to obtain the minimum and maximum reversible strain ε_{rev}, depend little on the initial chemical composition and are equal to 30 and 300 MPa, respectively. The coefficient $d\varepsilon_{rev}/d\sigma_{app}$, describing the growth of strain with applied stress, is equal to $7.2 \cdot 10^{-3}$ and $5.5 \cdot 10^{-3}$ MPa^{-1} in Ti-50.7at.%Ni crystals and Ti-51.7at.%Ni, respectively. Noticeable difference was observed in the maximum reversible strain: $\varepsilon_{rev} = 2.7\%$ and $\varepsilon_{rev} = 1.7\%$ for Ti-50.7at.%Ni and Ti-51.7at.%Ni crystals, respectively.

The dependence of the forward MT interval, $\Delta_1^\sigma = M_s^\sigma - M_f^\sigma$, and the reverse MT interval, $\Delta_2^\sigma = A_f^\sigma - A_s^\sigma$, on the applied compressive stresses, σ_{app}, are presented on Fig. 2c, d. These dependences are very different in the aged Ti-50.7at.%Ni and Ti-51.7at.%Ni crystals. In the Ti-50.7at.%Ni single crystals, the intervals Δ_1^σ and Δ_2^σ gradually increase with increasing σ_{app} from 20–30 to 6–23 K, respectively. In contrast, in Ti-51.7at.%Ni single crystals, the reverse MT interval, Δ_2^σ, is practically independent of stress and is equal to 17–21 K, while the forward MT interval, Δ_1^σ, sharply decreases (by more than 3 times) from 83 K at 50 MPa to 27 K at 250 MPa and then remains constant. Thus, asymmetric ε(T) curves were observed in the aged single crystals at low applied stresses. This effect was most pronounced in Ti-51.7at.%Ni crystals, where the values of Δ_1^σ and Δ_2^σ at 50 MPa differed by 60 K, while in Ti-50.7at.%Ni single crystals, Δ_1^σ and Δ_2^σ differed by only 15 K.

Table 1 MT temperatures for aged Ti-50.7at.%Ni and Ti-51.7at.%Ni single crystals

Chemical composition	MT temperatures								
	M_s, (± 2) K	M_f, (± 2) K	A_s, (± 2) K	A_f, (± 2) K	T_R, (± 2) K	T_R^{rev}, (± 2) K	Δ_1^0, (± 2) K	Δ_2^0, (± 2) K	ΔT_1^0, (± 2) K	ΔT_2^0, (± 2) K
Aged Ti-50,7at.%Ni	255	219	253	280	265	283	36	27	25	34
Aged Ti-51,7at.%Ni	235	148	250	268	263	273	87	18	33	102

Two hysteresis values, $\Delta T_1^\sigma = A_f^\sigma - M_s^\sigma$ and $\Delta T_2^\sigma = A_s^\sigma - M_f^\sigma$, were measured because of the asymmetric shape of the ε(T) curves (Fig. 2e, f). In aged Ti-50.7at.%Ni single crystals, the hysteresis ΔT_2^σ did not depend on the stress and equalled 20 K, while the hysteresis ΔT_1^σ decreased from 40 to 20 K with increasing stress. In aged Ti-51.7at.%Ni single crystals, the hysteresis ΔT_2^σ decreased from 40 to 20 K, while the hysteresis ΔT_1^σ decreased from 100 to 20 K.

Discussion

The Mechanism of Martensite Nucleation and Propagation During Stress-Free Cooling in Aged Ti-50.7at.%Ni and Ti-51.7at.%Ni Single Crystals

The mechanisms of martensite formation upon stress-free cooling in aged Ti-50.7at.%Ni and Ti-51.7at.%Ni crystals are similar and determined by large semi-coherent Ti_3Ni_4 particles. The main feature is the appearance of B19′-martensite near the particles, the boundaries of which are the sites of predominant nucleation [8, 18, 21]. This occurs because the barrier to martensite nucleation decreases due to the stress fields from the Ti_3Ni_4 particles, possible dislocations at the particle–matrix interface, and low Ni content in a local region near the particles. However, the different volume fractions of particles (11 and 22%) and different interparticle distances (300–500 nm and 50–150 nm) determine the formation and propagation of martensite and its morphology in Ti-50.7at.%Ni and Ti-51.7at.%Ni single crystals. In the aged Ti-50.7at.%Ni crystals with large interparticle distances, martensite appeared first near the particles and then in the interparticle regions, as observed in [22–24]. It is important to note that the interparticle regions are large and connected, so martensite can propagate from one region to another.

In aged Ti-51.7at.%Ni crystals, the following differences from Ti-50.7at.%Ni were noted. First, the four Ti_3Ni_4 particle variants with large volume fractions divided the B2-matrix into small regions completely separated from each other, similar to [9]. Therefore, martensite cannot propagate from one such region to another, and an MT occurs in separate interparticle regions due to the nucleation of the martensite crystals and increasing in the sizes.

Second, in the Ti-51.7at.%Ni crystals, the martensite nucleation did not occur simultaneously in all interparticle regions. The microstructure obtained in Ti-51.7at.%Ni single crystals was similar to a submicrocrystalline TiNi alloy, where grain boundaries limited the growth of martensite crystals and simultaneously served as martensite nucleation sites. For nanocrystalline TiNi alloys [25–27], decreasing the grain size from 600 to 100 nm led to a significant decrease

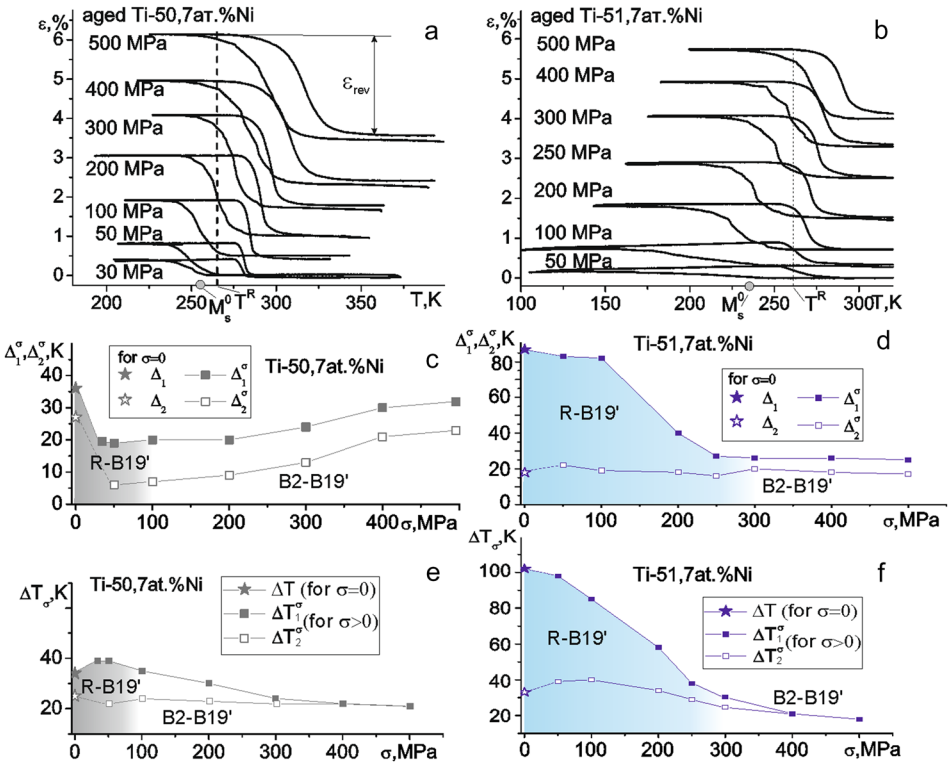

Fig. 2 The ε(T) curves for aged **a** Ti-50.7at.%Ni and **b** Ti-51.7at.%Ni crystals at stress-assisted cooling/heating cycles; **c**, **d** dependence of forward MT interval, Δ_1^σ, reverse MT interval, Δ_2^σ, and **e**, **f** thermal hysteresis, ΔT_1^σ and ΔT_2^σ, on applied stresses σ_{app}

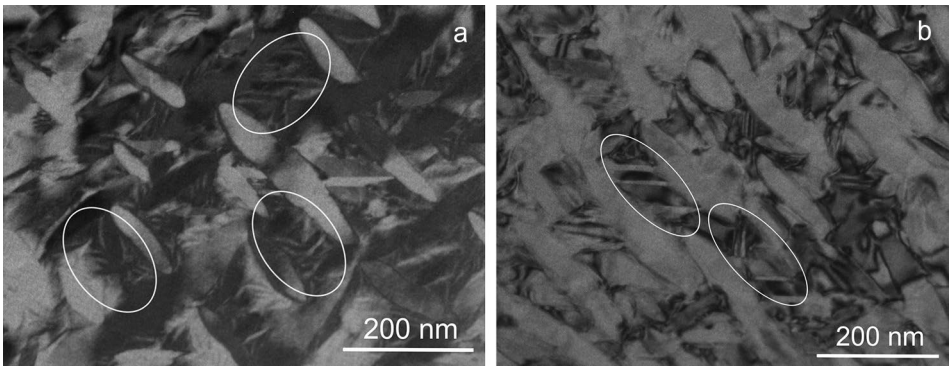

Fig. 3 Microstructure of the aged Ti-51.7at.%Ni single crystals: several variants of **a** thermal-induced R-martensite, **b** one variant of thermal-induced R-martensite

in MT temperatures, including the suppression of the B19′-transformation in grains smaller than 60 nm and suppression of the R-transformation in grains smaller than 30 nm. Thus, in large (150 nm) interparticle regions, MT began at higher temperatures than in small (less than 100 nm) interparticle regions. At a very small distance between particles of 50 nm or less, the MT can be suppressed. Thus, in Ti-51.7at.%Ni crystals, the MT during cooling proceeded by retraction into the transformation process of different B2-regions.

Third, in aged Ti-51.7at.%Ni single crystals, the number of variants of thermal-induced martensite depends on the size of the interparticle region (Fig. 3). In the 150-nm interparticle regions, various twinned variants of R-martensite generated by neighbouring particles (Fig. 3a), whereas, in regions smaller than 100 nm in size, one twinned version of R-martensite was observed in accordance with the internal stress fields from the particles (Fig. 3b). Similar morphologies have been observed by Waitz and Karnthaler, where only one twinned variant of martensite was found in polycrystals with a grain size of less than 100 nm [27–29].

The features of the microstructure that determined the heterogeneous nucleation and growth of martensite in aged Ti-51.7at.%Ni crystals led to a wide temperature range of forward R-B19′ MT upon stress-free cooling, $\Delta_1^0 = M_s^0 - M_f^0 = 87$ K, in contrast to Ti-50.7at.%Ni crystals, where the MT interval, $\Delta_1^0 = M_s^0 - M_f^0 = 36$ K, was 2.5 times smaller.

MT During Stress-Assisted Cooling in Aged Ti-50.7at.%Ni and Ti-51.7at.%Ni Single Crystals

At Stresses $\sigma_{app} < 100$ MPa

The interval Δ_1^σ of the forward R-B19′ MT during cooling under a small stress ($\sigma_{app} < 100$ MPa) effectively did not change compared to stress-free cooling (Fig. 2b–d). In Ti-50.7at.%Ni crystals, the forward MT interval, Δ_1^σ, is 4 times smaller than in Ti-51.7at.%Ni crystals, where $\Delta_1^\sigma > 80$ K. The forward MT interval during stress-assisted cooling is determined by the following factors: structural inhomogeneity, elastic and dissipated energies, and temperature dependence of the lattice parameters of the R-phase.

The mechanisms of martensite nucleation and propagation during cooling under low stresses ($\sigma_{app} < 100$ MPa) were similar to that during stress-free cooling. In aged Ti-50.7at.%Ni single crystals with large interparticle distances, martensite first appeared near the particles and then in the interparticle regions, where martensite can propagate from one region to another. In aged Ti-51.7at.%Ni single crystals, the MT occurred similar to during stress-free cooling by the gradual retraction into the transformation process of B2-regions with different sizes (described above in Sect. "The Mechanism of Martensite Nucleation and Propagation During Stress-Free Cooling in Aged Ti-50.7at.%Ni and Ti-51.7at.%Ni Single Crystals"). The difference between the morphology of stress-assisted and stress-free cooling is as follows. Internal stress fields from the semi-coherent Ti_3Ni_4 particles can reach 280 MPa [30]. Hence, the applied stress $\sigma_{app} < 100$ MPa was insufficient to overcome the internal stress fields from the particles and form a completely oriented martensite. Therefore, a mixture of B19′-martensite variants arose under the superposition of stress fields from particles and external applied stresses $\sigma_{app} < 100$ MPa. This mechanisms is fair for Ti-50.7at.%Ni and Ti-51.7at.%Ni. But the particle volume fraction in Ti-51.7at.%Ni single crystals was larger, than in Ti-50.7at.%Ni single crystals, so their contribution to the superposition of stress fields was greater.

Other factors affecting the interval Δ_1^σ are the elastic ΔG_{rev} and dissipated ΔG_{irr} energies. According to [31], by using the equation balancing the chemical ΔG_{ch} and non-chemical ΔG_{nonch} components of free energy, one can obtain an expression for the MT temperatures:

$$M_s^\sigma = T_0 - \frac{|\Delta G_{rev}(0)|}{\Delta S_{ch}} - \frac{|\Delta G_{irr}(0)|}{\Delta S_{ch}},$$
$$M_f^\sigma = T_0 - \frac{|\Delta G_{rev}(1)|}{\Delta S_{ch}} - \frac{|\Delta G_{irr}(1)|}{\Delta S_{ch}}$$

$$A_s^\sigma = T_0 - \frac{|\Delta G_{rev}(1)|}{\Delta S_{ch}} + \frac{|\Delta G_{irr}(1)|}{\Delta S_{ch}},$$
$$A_f^\sigma = T_0 - \frac{|\Delta G_{rev}(0)|}{\Delta S_{ch}} + \frac{|\Delta G_{irr}(0)|}{\Delta S_{ch}} \quad (1)$$

Here $\Delta G_{rev}(0)$ and $\Delta G_{irr}(0)$ are the elastic dissipated energies at the beginning of MT at volume fraction of oriented martensite equal to 0, $\Delta G_{rev}(0)$ and $\Delta G_{irr}(0)$ at the finish of MT at volume fraction of oriented martensite equal to 1. Then, the forward MT interval can be expressed as:

$$\Delta_1^\sigma = M_s^\sigma - M_f^\sigma = \frac{1}{\Delta S_{ch}}\big(|\Delta G_{rev}(1)| - |\Delta G_{rev}(0)| + |\Delta G_{irr}(1)| - |\Delta G_{irr}(0)|\big). \quad (2)$$

The aged single crystals contained dispersed particles, and, hence, the elastic energy ΔG_{rev} was generated in the material during the nucleation of the first martensite plate. Therefore, $\Delta G_{rev}(0) \neq 0$. In addition, in this case, the hysteresis (and the dissipated energy, ΔG_{irr}) depends on the volume fraction of oriented martensite, as can be seen from Fig. 2, so $\Delta G_{irr}(0) \neq \Delta G_{irr}(1)$.

In the Ti-51.7at.%Ni single crystals, the contributions from the elastic and dissipated energies were greater than in the Ti-50.7at.%Ni crystals, which can be explained as follows. In Ti-51.7at.%Ni single crystals, a high density of compound twins $(001)_{B19'}$ was observed due to small interparticle distances. Composite twins appeared near particles in places of high elastic lattice distortions, and they are the geometrically necessary twins to maintain the continuity of the particle and matrix [27, 32]. According to the gradient theory of plasticity [23, 33, 34,], the density of twins, ρ_{tw}, increases with decreasing interparticle distances, λ:

$$\rho_{tw} = \frac{1}{b} \bullet \frac{\gamma}{\lambda}, \quad (3)$$

where b is the Burgers vector of compound twins $<100>\{001\}$, γ is the martensitic shear, and λ is the interparticle distances. The high density of compound twins led to a high stored elastic energy during the transformation and, hence, high value of ΔG_{rev} in Ti-51.7at.%Ni crystals compared to Ti-50.7at.%Ni crystals. The dissipated energy can be estimated from the hysteresis value. Based on expression (1), the hysteresis ΔT_1^σ and ΔT_2^σ can be written as:

$$\Delta T_1^\sigma = A_f^\sigma - M_s^\sigma = \frac{2}{\Delta S_{ch}}|\Delta G_{irr}(0)|, \quad (4)$$

$$\Delta T_2^\sigma = A_s^\sigma - M_f^\sigma = \frac{2}{\Delta S_{ch}}|\Delta G_{irr}(1)|. \quad (5)$$

At $\sigma_{app} < 100$ MPa, the hysteresis ΔT_2^σ was 2.5 times greater in the Ti-51.7at.%Ni single crystals, than in the

Ti-50.7at.%Ni crystals. In addition, in the Ti-51.7at.%Ni single crystals, the hysteresis ΔT_2^σ was 60 K greater than the hysteresis ΔT_1^σ, indicating a strong increase in the dissipated energy, ΔG_{irr}, with increasing volume fraction of martensite. In contrast, in the Ti-50.7at.%Ni single crystals, ΔT_σ^2 exceeded ΔT_1^σ by only 18 K, indicating that the change in the dissipated energy during the MT is small.

In Ti-51.7at.%Ni single crystals, the hysteresis ΔT_1^σ and ΔT_2^σ are different at $\sigma_{app} < 100$ MPa, because a significant overheating, $\Delta A_s^\sigma = \Delta T_2^\sigma - \Delta T_1^\sigma$, is required to start the reverse MT. Similar asymmetric curves were observed in [15, 22] for aged TiNi single crystals because of the high energy barrier for starting the reverse MT. This barrier can be associated with the difficult disappearance of B19′-martensite with a high density of $(001)_{B19'}$ twins, which do not form an invariant habit plane between austenite and martensite. When the asymmetric ε(T) curves were observed, a forward MT occurs from the R-phase into B19′-martensite. However, the reverse MT can occur along the path B19′-R-B2 (or even directly from B19′ to B2) and the temperature A_f^σ at $\sigma_{app} < 100$ MPa coincided with the temperature T_R^{rev}. Different sequence of MT at forward and reverse MT also can be a reason for asymmetric ε(T) curves.

At Stresses 100 MPa < σ_{app} < 300 MPa

In the stress range of 100 MPa < σ_{app} < 300 MPa, the reversible strain reached maximum values in Ti-50.7at.%Ni and Ti-51.7at.%Ni single crystals. Simultaneously, the morphology of the martensite changed. High external stresses (300 MPa and higher) exceeded the internal stress fields from the particles and allowed the formation of the maximum fraction of oriented martensite. In Ti-50.7at.%Ni single crystals the interval Δ_1^σ of forward R-B19′ MT did not change with increasing applied stress up to 300 MPa. In contrast, in Ti-51.7at.%Ni single crystals, an increase in the stress σ_{app} above 100 MPa led to a decrease in the interval Δ_1^σ of forward R-B19′ MT from 83 K at 50 MPa to 27 K at 330 MPa (Fig. 2).

The reasons for the decrease in the interval Δ_1^σ in single crystals Ti-51.7at.%Ni were as follows. First, the processes driving the retraction of various interparticle regions into the R-B19′ transformation could change. The increase in the applied stresses led to an increase in the temperature M_s^σ according to the Clausius–Clapeyron equation [18]. The MT start temperatures in various local interparticle regions, M_s^σ(lok), could increase with different growth coefficients. Thus, if at low stress $\sigma_{app} < 100$ MPa MT occurred in interparticle regions at different temperatures, then at high stresses $\sigma_{app} > 100$ MPa MT can occur at the same temperatures in interparticle regions of different size. This may be one of the reasons for the reduction in the forward MT interval.

Second, the change in the rhombohedricity of the R-phase (that is, the change in the lattice parameter) should be took into account, considering the reasons for the change in the forward MT interval, Δ_1^σ. As shown in [35–37], the angle of the R-phase unit cell decreased from $\alpha = 90°$ to 89.3° with a decrease in temperature from T_R to $T_R - 20$ K. Because the Ti_3Ni_4 particles grew in the B2-phase, a change in the rhombohedricity of R-martensite led to a change in the dimensional mismatch parameters between the lattices of the R-martensite and the Ti_3Ni_4 particles. Consequently, a large mismatch between the lattices of the R-phase and particles was observed at low stresses $\sigma_{app} < 100$ MPa, when the transformation occurred at low temperatures ($M_s^\sigma = 244$ K and $M_f^\sigma = 155$ K were less than T_R by 20 and 110 K, respectively). Simultaneously, the resistance force obstructive the movement of the interphase boundary and the dissipative energy are large. The MT temperatures increased with increasing applied stresses: at $\sigma_{app} = 300$ MPa, $M_s^\sigma = T_R$ and $M_f^\sigma = 235$ K (less than T_R by 30 K). These changes decreased the mismatch between the lattices of R-martensite and Ti_3Ni_4 particles. Then, the resistance force obstructive the movement of the interphase boundary and the dissipative energy started to increase significantly. Consequently, the change in the R-phase rhombohedricity also affected the reduction of the thermal hysteresis, ΔT_2^σ.

The effect of R-phase rhombohedricity on the forward MT interval, Δ_1^σ, and the hysteresis, ΔT_2^σ, could be stronger in the Ti-51.7at.%Ni single crystals because, first, the temperature difference ($M_s^\sigma - T_R$) is greater (28 K) than in the Ti-50.7at.%Ni single crystals (10 K). When the temperature M_s^σ increased with increasing stresses, the difference ($M_s^\sigma - T_R$) decreased because the temperature T_R almost does not depend on the stress [8, 15, 18]. The Ti-51.7at.%Ni single crystals required increasing the stress up to 300 MPa to reduce the difference ($M_s^\sigma - T_R$) down to zero, whereas the Ti-50.7at.%Ni single crystals required increasing the stress to only 100 MPa. Second, the increase in the nickel-concentration leads to an increase in rhombohedral distortion of the R-phase lattice [38]. So, the describing effect, namely the reduction of interval Δ_1^σ with increasing applied stress (and increasing M_s^σ temperature) associated with the change of mismatch parameters between the lattices of the R-martensite and the Ti_3Ni_4 particles will intensify in Ti-51.7at.%Ni.

At Stresses $\sigma_{app} > 300$ MPa

Increasing stress affected not only the forward MT interval, Δ_1^σ, but also led to overheating during reverse MT, $\Delta A_s^\sigma = \Delta T_2^\sigma - \Delta T_1^\sigma$. In other words, the reverse MT start temperature, A_s^σ, decreased by ΔA_s^σ. As a result, the ε(T) curves became symmetric; that is, the thermal hysteresis did not depend on the martensite volume fraction $\Delta T_1^\sigma = \Delta T_2^\sigma$. In this case, the forward MT occurred directly from the B2-phase to the B19′-martensite, and the reverse MT occurred in an inverse manner from the B19′-martensite to the B2-phase. In Ti-50.7at.%Ni single crystals, this occurred at stresses above 100 MPa, and above 300 MPa in Ti-51.7 at.% Ni single crystals. At this stresses, the thermal hysteresis did not change with increasing stress in both single crystals and can be described using the Roitburd model [36]. The Schmid factor for detwinning of B19′-martensite under compression along the [001]-direction is zero [3, 15, 18]. Therefore, according to [36], an increase in stress does not affect the twin structure of B19′-martensite or the dissipated energy, ΔG_{irr}, and, consequently, the hysteresis. Based on the Roitburd model, such a description can be used if there is no influence from other factors.

In the Ti-50.7at.%Ni and Ti-51.7at.%Ni single crystals, the maximum reversible strain is achieved at stress $\sigma_{app} > 300$ MPa. The values differed: $\varepsilon_{rev} = 2.7\%$ and $\varepsilon_{rev} = 1.7\%$ for Ti-50.7at.%Ni and Ti-51.7at.%Ni single crystals, respectively. The maximum reversible strain is determined by the following parameters. First is the theoretical value of the lattice strain during B2–B19′ MT under compression along the [001]-direction. As shown in [8, 15, 18], in TiNi alloys, the theoretical lattice strain is 4.4%. In aged single crystals, the decrease in strain is associated with dendrites and untransformed areas of austenite, as evidenced by the small strain of 2.8% in quenched single crystals (see Sect. "MT During Stress-Assisted Cooling in Aged Ti-50.7at.%Ni and Ti-51.7at.%Ni Single Crystals" and study [1]). Second, the theoretical lattice strain ε_0^* in aged alloys is determined by the volume fraction of the matrix undergoing the MT and differ from the theoretical lattice strain ε_0 in single-phase alloys: $\varepsilon_0^* = \varepsilon_0 - \varepsilon_0\,\delta$ (δ is the volume fraction of the particles). In aged Ti-51.7at.%Ni single crystals, the volume fraction of particles (22%) was 2 times larger than in Ti-50.7at.%Ni crystals (11%). Consequently, the volume fractions of the matrix undergoing the MT were different in these crystals. This is the main reason for the different reversible strains observed experimentally. Third, in Ti-51.7at.%Ni single crystals, small interparticle distances (less than 100 nm) can lead to the formation of one martensite variant, oriented in accordance with the internal stress fields from particles and differing from the main oriented martensite induced by external stress. If the external stress does not reorient this martensite variant, then it can make a small contribution to the transformation strain, reducing the amount of reversible strain. Fourth, the formation of B19′ martensite is suppressed at interparticle distances of less than 50 nm, as shown in [27–29].

The Effect of Aging on the Dependence of SME Parameters on the Chemical Composition Compared with Single-Phase Quenched Crystals

The dependences $\varepsilon_{rev}(\sigma_{app})$ in aged crystals should be considered in comparison with quenched crystals (Fig. 4), which were studied in detail in our previous work [1]. Such analysis clarifies the effect of aging on the dependence of SME parameters on chemical composition.

Figure 4a shows that the $\varepsilon_{rev}(\sigma_{app})$ plots of quenched crystals strongly depend on the chemical composition, which is determined by the type of transition (thermal-induced MT or strain glass transition). In quenched Ti-50.7at.%Ni single crystals, a mixture of self-accommodating martensite variants and oriented martensite has been found to form during thermal cycles under stress $\sigma_{app} < \sigma_{max}$ [1, 2]. This process required a very low stress of $\sigma_{min} = 50$ MPa. The increase in strain with increasing stress occurred due to the gradual rearrangement of the mixture structure, that is, an increase in the volume fraction of oriented martensite, which explains the low strain growth coefficient $d\varepsilon_{rev}/d\sigma = 6.2 \cdot 10^{-3}$ MPa^{-1}. In quenched Ti-51.7at.%Ni single crystals, where the strain glass transition occurred, the self-accommodating martensite structure did not form; therefore, such a mixture did

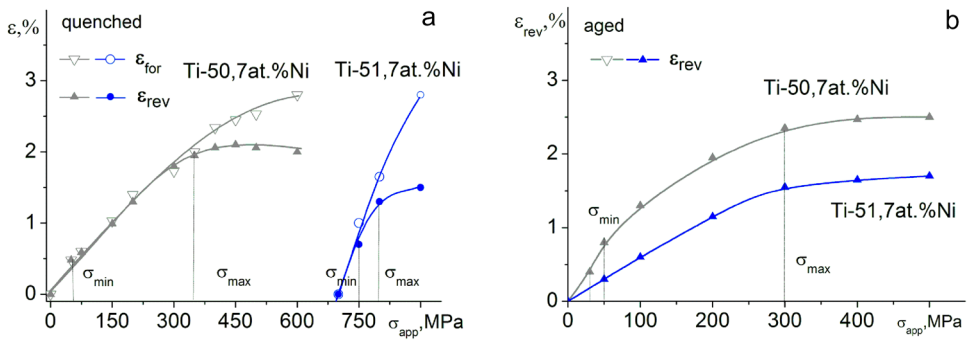

Fig. 4 Dependence of reversible strain, ε_{rev}, on applied compressive stress σ_{app} for quenched **a** Ti-50.7at.%Ni and **b** Ti-51.7at.%Ni single crystals. Data (a) was taken from [1]

not arise. Only oriented martensite appeared in quenched Ti-51.7at.%Ni single crystals, which required an extremely high stress σ_{min} = 750 MPa, 15 times higher than in Ti-50.7at.%Ni crystals. In this case, a small increase in the applied stress above σ_{min} (by 150 MPa) was sufficient for maximum strain. Therefore, in quenched Ti-51.7at.%Ni crystals, the strain growth coefficient $d\varepsilon_{rev}/d\sigma = 18.6 \cdot 10^{-3}$ MPa^{-1} 3 times bigger than in quenched Ti-50.7at.%Ni single crystals.

The strong dependence of the $\varepsilon_{rev}(\sigma_{app})$ plots on the chemical composition in quenched crystals degenerated after aging. In the aged single crystals, the $\varepsilon_{rev}(\sigma_{app})$ plots have similar forms (Fig. 4). The values of σ_{min} and σ_{max} stresses were close. The values of the strain growth coefficient, $d\varepsilon_{rev}/d\sigma$ were differed only in 1.3 times (against 3 times in quenched crystals). The weak dependence of the $\varepsilon_{rev}(\sigma_{app})$ plots on the initial chemical composition in aged crystals was associated with the following changes. First, the particle precipitation reduced the Ni content and induced the thermal-induced MTs in aged Ti-51.7at.%Ni single crystals. That is why the stress σ_{min} decreased significantly by 15 times (from 750 to 50 MPa), and the stress σ_{max} decreased by 2.5 times (from 800 to 300 MPa) after aging in Ti-51.7at.%Ni single crystals. Moreover, the strain growth coefficient, $d\varepsilon_{rev}/d\sigma$, decreased by 3 times (from $18.6 \cdot 10^{-3}$ to $5.5 \cdot 10^{-3}$ MPa^{-1}). In contrast, in the Ti-50.7at.%Ni single crystals, thermal-induced MTs with the formation mixture of self-accommodating martensite variants and oriented martensite were observed before and after aging, respectively. Therefore, in these crystals, the aging had a small effect on the $\varepsilon_{rev}(\sigma_{app})$ plots: the σ_{min} and σ_{max} stresses changed slightly, and the $d\varepsilon_{rev}/d\sigma$ coefficients were close ($6.2 \cdot 10^{-3}$ MPa^{-1} in quenched and $7.2 \cdot 10^{-3}$ MPa^{-1} in aged crystals).

Second, the similar shapes of the $\varepsilon_{rev}(\sigma_{app})$ plots after aging are associated with similar chemical compositions of the matrixes in the aged Ti-50.7at.%Ni and Ti-51.7at.%Ni crystals. As presented in [5, 6], alloys with different Ni content (from 50.6 to 51.5at.%) became 50.4–50.6at.% after aging. This effect occurred due to the different volume fractions of precipitating particles. The higher the Ni content, the greater the particle volume fraction and the greater the reduction in the Ni content in the matrix.

Third, the weakening dependence of the $\varepsilon_{rev}(\sigma_{app})$ plots on the chemical composition after aging can be associated with the changing in mechanisms of B19′-martensite formation in quenched and aged crystals. In quenched Ti-50.7at.%Ni and Ti-51.7at.%Ni crystals, the mechanisms of B19′-martensite formation are completely different, whereas they are similar in the aged crystals. The mechanism was determined by large semi-coherent Ti_3Ni_4 particles and was valid for aged Ti-50.7at.%Ni and Ti-51.7at.%Ni crystals (see Sect. "The Mechanism of Martensite Nucleation and Propagation During Stress-Free Cooling in Aged Ti-50.7at.%Ni and Ti-51.7at.%Ni Single Crystals"). Its main feature is the occurrence of B19′-martensite near the particles, whose boundaries are the sites of predominant nucleation of martensite and simultaneously limit the growth of martensite crystals [5, 8, 21]. Despite the features, discussed in Sects. "The Mechanism of Martensite Nucleation and Propagation During Stress-Free Cooling in Aged Ti-50.7at.%Ni and Ti-51.7at.%Ni Single Crystals" and "MT During Stress-Assisted Cooling in Aged Ti-50.7at.%Ni and Ti-51.7at.%Ni Single Crystals", the mixtures of B19′-martensite variants formed during stress-assisted cooling in aged single crystals are similar. In both aged single crystals the mixtures of B19′-martensite variants were formed under stress-assisted cooling. These mixtures were formed from the R-phase or B2-phase under the superposition of stress fields from the particles and external applied stresses. The evolution of the martensite mixtures with increasing stress σ_{app} caused an increase in strain ε_{rev}. Therefore, in aged Ti-50.7at.%Ni and Ti-51.7at.%Ni crystals, close values of $d\varepsilon_{rev}/d\sigma$ coefficients and σ_{min} and σ_{max} stresses were observed.

Thus, if the dependence of the SME on the chemical composition in the quenched crystals is determined by the type of transition (thermal-induced MT or strain glass transition), then in the aged crystals it is determined by the different volume fractions of Ti_3Ni_4 particles and different interparticle distances. In the quenched crystals, different types of transition led to completely different $\varepsilon_{rev}(\sigma_{app})$ plots, but at the same time, the ε(T) curves were symmetric and characterised by a close values of strains, forward MT intervals, Δ_1^{σ}, and thermal hysteresis, ΔT^{σ} [1]. In contrast, in the aged crystals, the different volume fractions of Ti_3Ni_4 particles and interparticle distances had little effect on the σ_{min} and σ_{max} stresses and $d\varepsilon_{rev}/d\sigma$ coefficient; however, they strongly affected the reversible strain, ε_{rev}, forward MT intervals, Δ_1^{σ}, and thermal hysteresis, $\Delta T_1^{\sigma} = A_f^{\sigma} - M_s^{\sigma}$ and $\Delta T_2^{\sigma} = A_s^{\sigma} - M_f^{\sigma}$.

Conclusions

The SME in thermal cycles under compression in [001]-oriented Ti-50.7at.%Ni and Ti-51.7 at.%Ni single crystals aged at 823 K for 1 h was studied. During aging, Ti_3Ni_4 particles with sizes of 300–400 nm, a volume fraction of 11 and 22%, and interparticle distances of 300–500 nm and 50–150 nm were precipitated. Based on the results, we reached the following conclusions:

- In the aged single crystals, the SME parameters were determined by the volume fraction of particles and interparticle distances, unlike the quenched single crystals, in which the SME parameters were determined by the type of transition (thermal-induced MT in Ti-50.7at.%Ni or strain glass transition in Ti-51.7at.%Ni crystals);

- Aging led to a strong degeneration of the $\varepsilon_{rev}(\sigma_{app})$ plots on the chemical composition, which was typical for the quenched crystals. In aged Ti-50.7at.%Ni and Ti-51.7at.%Ni single crystals, close values of the σ_{min} (30 MPa) and σ_{max} (300 MPa) stresses, necessary to achieve the minimum and maximum reversible strain ε_{rev}, were observed, and similar values (differed in 1.3 times) for the strain growth coefficient $d\varepsilon_{rev}/d\sigma$ were obtained. These parameters are close because of the similar chemical composition of the matrix after the precipitation of Ti_3Ni_4 particles and the similar morphology of martensite in aged crystals in contrast to the quenched ones. In contrast, in quenched Ti-50.7at.%Ni and Ti-51.7at.%Ni crystals, the stress σ_{min} differed by a factor of 15, the stress σ_{max} differed by a factor of 2, and the coefficient $d\varepsilon_{rev}/d\sigma$ by a factor of 3.
- The following SME parameters not depending on the chemical composition of the quenched single crystals but differed greatly after aging were established: the reversible strain ε_{rev}, the forward MT interval, Δ_1^{σ}, and thermal hysteresis, $\Delta T_1^{\sigma} = A_f^{\sigma} - M_s^{\sigma}$ and $\Delta T_2^{\sigma} = A_s^{\sigma} - M_f^{\sigma}$. These features of SME in the aged single crystals were determined by the different volume fraction of particles and the change in the conditions for the nucleation and growth of B19′-martensite crystals with a decrease in interparticle distance from 500 to 50 nm.

Acknowledgements This research was funded by the Project No. 0721-2020-0022 and Program "Priority-2030".

Data availability The raw/processed data required to reproduce these findings cannot be shared at this time as the data also forms part of an ongoing study.

References

1. Timofeeva EE, Panchenko EYu, Zherdeva MV, Eftifeeva AS, Surikov NYu, Tagiltsev AI, Fatkullin I, Tokhmetova A, Yanushonite EI, Chumlyakov YuI (2022) Shape memory effect in TiNi single crystals with thermal-induced martensite transformation or strain glass transition. J Alloys Compd 922:166275
2. Timofeeva EE, Panchenko EYu, Surikov NYu, Tagiltsev AI, Marchenko ES, Chumlyakov YuI (2022) On the stress-temperature dependences in TiNi-based shape memory alloys. J Alloys Compd 905:164227
3. Sehitoglu H, Jun J, Zhang X, Karaman I, Chumlyakov Y, Maier HJ, Gall K (2001) Shape memory and pseudoelastic behavior of 51.5%Ni–Ti single crystals in solutionized and overaged state. Acta Mater 49:3609–3620
4. Karaca HE, Kaya I, Tobe H, Basaran B, Nagasako M, Kainuma R, Chumlyakov Y (2013) Shape memory behavior of high strength Ni54Ti46 alloys. Mater Sci Eng A 580:66–70
5. Yang Z, Tirry W, Schryvers D (2005) Analytical TEM investigations on concentration gradients surrounding Ni_4Ti_3 precipitates in Ni–Ti shape memory material. Scr Mater 52:1129–1134
6. Schryvers D, Tirry W, Yang ZQ (2006) Measuring strain fields and concentration gradients around Ni_4Ti_3 precipitates. Mater Sci Eng A 438–440:485–488
7. Chumlyakov YuI, Efimenko SP, Kireeva IV, Panchenko EYu, Sehitogly H, Gall K, Yahia LH (2001) Effects of shape memory and superelasticity in aged TiNi single crystals. Dokl Phys 46:849–852
8. Otsuka K, Ren X (2005) Physical metallurgy of Ti–Ni-based shape memory alloys. Prog Mater Sci 50:511–678
9. Timofeeva EE, Surikov NYu, Tagiltsev AI, Eftifeeva AS, Neyman AA, Panchenko EYu, Chumlyakov YuI (2020) The superelasticity and shape memory effect in Ni-rich Ti-51.5Ni single crystals after one-step and two-step ageing. Mater Sci Eng A 796:140025
10. Hamilton RF, Sehitoglu H, Chumlyakov Y, Maier HJ (2004) Stress dependence of the hysteresis in single crystal NiTi alloys. Acta Mater 52:3383–3402
11. Fan G, Chen W, Yang S, Zhu J, Ren X, Otsuka K (2004) Origin of abnormal multi-stage martensitic transformation behavior in aged Ni-rich Ti–Ni shape memory alloys. Acta Mater 52:4351–4362
12. Kang J, Li R, Zheng D, Wu H, Wang M, Niu P, Li J, Liu X, Lai D, Yuana T (2023) Unconventional precipitation and martensitic transformation behaviour of Ni-rich NiTi alloy fabricated via laser-directed energy deposition. Virtual Phys Prototyp 18:2231415
13. Khalil-Allafi J, Dlouhy A, Eggeler G (2002) Ni_4Ti_3-precipitation during aging of NiTi shape memory alloys and its influence on martensitic phase transformations. Acta Mater 50:4255–4274
14. Ryklina EP, Polyakova KA, Tabachkova NYu, Resnina NN, Prokoshkin SD (2018) Effect of B2 austenite grain size and aging time on microstructure and transformation behavior of thermomechanically treated titanium nickelide. J Alloys Compd 764:626–638
15. Kaya I, Karaca HE, Souri M, Chumlyakov Y, Kurkcu H (2017) Effects of orientation on the shape memory behavior of $Ni_{51}Ti_{49}$ single crystals. Mater Sci Eng A 686:73–81
16. Stebner AP, Bigelow GS, Yang J, Shukla DP, Saghaian SM, Rogers R, Garg A, Karaca HE, Chumlyakov Y, Bhattacharya K, Noebe RD (2014) Transformation strains and temperatures of a nickel–titanium–hafnium high temperature shape memory alloy. Acta Mater 76:40–53
17. Evirgen A, Karaman I, Santamarta R, Pons J, Noebe RD (2015) Microstructural characterization and shape memory characteristics of the $Ni_{50.3}Ti_{34.7}Hf_{15}$ shape memory alloy. Acta Mater 83:48–60
18. Chumlyakov YI, Kireeva IV, Panchenko EY, Timofeeva EE, Kretinina IV, Kuts OA (2015) Physics of thermoelastic martensitic transformation in high-strength single crystals. Mater Sci Found 81–82:107–173
19. Miyazaki S, Wayman CM (1988) The R-phase transition and associated shape memory mechanism in Ti-Ni single crystals. Acta Metall 36:181–192
20. Miyazaki S, Kimura S, Otsuka K (1998) Shape-memory effect and pseudoelasticity associated with the R-phase transition in Ti-50.5at.%Ni single crystals. Philos Mag A 57:467–478
21. Michutta J, Somsen Ch, Yawny A, Dlouhy A, Eggeler G (2006) Elementary martensitic transformation processes in Ni-rich NiTi single crystals with Ni_4Ti_3 precipitates. Acta Mater 54:3525–3542
22. Panchenko EYu, Chumlyakov YuI, Maier H (2014) Features of multistage thermoelastic B2-R-B19′ martensitic transformations in heterophase single crystals of Ti–Ni alloys. Russ Phys J 57:1116–1125
23. Bataillard L, Bidaux J-E, Gotthardt R (1998) Interaction between microstructure and multiple-step transformation in binary NiTi alloys using in-situ transmission electron microscopy observations. Philosop Mag A 78:327–344

24. Li J-F, Zheng Z-Q, Li X-W, Li S-C (2009) Effect of compressive stress aging on transformation strain and microstructure of Ni-rich TiNi alloy. Mater Sci Eng A 523:207–213
25. Hornbogen E, Mertinger V, Wurzel D (2001) Microstructure and tensile properties of two binary NiTi-alloys. Scripta Mater 44:171–178
26. Zhang H, Li X, Zhang X (2012) Grain-size-dependent martensitic transformation in bulk nanocrystalline TiNi under tensile deformation. J Alloys Compd 544:19–23
27. Waitz T, Antretter T, Fischer FD, Simha NK, Karnthaler HP (2007) Size effects on the martensitic phase transformation of NiTi nanograins. J Mech Phys Solids 55:419–444
28. Waitz T, Pranger W, Antretter T, Fischer FD, Karnthaler HP (2008) Competing accommodation mechanisms of the martensite in nanocrystalline NiTi shape memory alloys. Mater Sci Eng A 481–482(1):479–483
29. Waitz T, Kazykhanov V, Karnthaler HP (2004) Martensitic phase transformations in nanocrystalline NiTi studied by TEM. Acta Mater 52:137–147
30. Tirry W, Schryvers D (2005) Quantitative determination of strain fields around Ni_4Ti_3 precipitates in NiTi. Acta Mater 53:1041–1049
31. Beke DL, Daroczi L, Samy NM, Toth LZ, Bolgar MK (2020) On the thermodynamic analysis of martensite stabilization treatments. Acta Mater 200:490–501
32. Waitz T (2005) The self-accommodated morphology of martensite in nanocrystalline NiTi shape memory alloys. Acta Mater 53:2273–2283
33. Fan QC, Zhang YH, Wang YY, Sun MY, Meng YT, Huang SK, Wen YH (2017) Influences of transformation behavior and precipitates on the deformation behavior of Ni-rich NiTi alloys. Mater Sci Eng A 700:269–280
34. Fleck NA, Muller GM, Ashby MF, Hutchinson JW (1994) Strain gradient plasticity: theory and experiment. Acta Metal Mater 42:475–487
35. Kim JI, Liu Y, Miyazaki S (2004) Ageing-induced two-stage R-phase transformation in Ti-50.9at.%Ni. Acta Mater 52:487–499
36. Roytburd AL, Slusker Ju (1995) Deformation through a coherent phase transformation. Scripta Metall Mater 32:761–766
37. Sittner P, Landa M, Lukas P, Novak V (2006) R-phase transformation phenomena in thermomechanically loaded NiTi polycrystals. Mech Mater 38:475–492
38. Prokoshkin SD, Korotitskiy AV, Brailovski V, Turenne S, Khmelevskaya IYu, Trubitsyna IB (2004) On the lattice parameters of phases in binary Ti–Ni shape memory alloys. Acta Mater 52:4479–4492